Reaction of Thin Films of Solid-State Benzene and Pyridine with Calcium

ARTICLE *in* JOURNAL OF THE AMERICAN CHEMICAL SOCIETY · JULY 2012

Impact Factor: 12.11 · DOI: 10.1021/ja3016186 · Source: PubMed

3 AUTHORS:

Dallas Matz
The University of Arizona
10 PUBLICATIONS **21** CITATIONS
SEE PROFILE

Matt Schalnat
General Atomics
10 PUBLICATIONS **106** CITATIONS
SEE PROFILE

Jeanne E Pemberton
The University of Arizona
175 PUBLICATIONS **4,748** CITATIONS
SEE PROFILE

JACS
JOURNAL OF THE AMERICAN CHEMICAL SOCIETY
Article
pubs.acs.org/JACS

Reaction of Thin Films of Solid-State Benzene and Pyridine with Calcium

Dallas L. Matz, Matthew C. Schalnat,† and Jeanne E. Pemberton*

Department of Chemistry and Biochemistry, University of Arizona, 1306 East University Boulevard, Tucson, Arizona 85721, United States

Supporting Information

ABSTRACT: The reaction between small organic molecules and low work function metals is of interest in organometallic, astronomical, and optoelectronic device chemistry. Here, thin, solid-state, amorphous benzene and pyridine films are reacted with Ca at 30 K under ultrahigh vacuum with the reaction progress monitored by Raman spectroscopy. Although both films react with Ca to produce product species identifiable by their vibrational spectroscopic signatures, benzene is less reactive with Ca than pyridine. Benzene reacts by electron transfer from Ca to benzene producing multiple species including the phenyl radical anion, the phenyl radical, and the benzyne diradical. Pyridine initially reacts along a similar electron transfer pathway as indicated by the presence of the corresponding pyridyl radical and pyridyne diradical species, but these pyridyl radicals are less stable and subject to further ring-opening reactions that lead to a complex array of smaller molecule reaction products and ultimately amorphous carbon. The elucidation of this reaction pathway provides insight into the reactions of aromatics with Ca that are relevant in the areas of catalysis, astrochemistry, and organic optoelectronics.

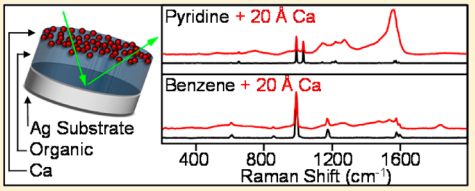

INTRODUCTION

The study of polycyclic aromatic hydrocarbons (PAHs) is important in the areas of petroleum chemistry, combustion, astrochemical, environmental, and optoelectronic device research, and reactions of such molecules and their derivatives with highly reactive Ca atoms have long been of interest to researchers in these fields. It is thought that PAHs form by reaction of small molecules in interstellar and circumstellar environments.[8,9] These include small molecules such as benzene and related species, both of which have been observed in protoplanetary nebulae.[10] Ca-rich environments have also been associated with PAH degradation to products such as graphite whiskers in both laboratory studies and in interstellar media.[11] Of note in environmental science, photocatalytic strategies utilizing various forms of Ca have been shown to facilitate degradation of highly toxic benzene pollutants to less toxic compounds, with especially high efficiency shown by $CaSb_2O_5(OH_2)$.[12]

The reaction of benzene with Ca has been of fundamental interest in organometallic chemistry, wherein Ca has been considered a "heavy Grignard" reagent that can undergo reactions similar to those of Mg, albeit to a much lesser extent.[13] DFT calculations by Fredriksson and co-workers[14] on the interaction of Ca atoms with benzene suggest that Ca atoms interact only weakly with benzene leaving the electronic structure of benzene unperturbed with no evidence for Ca−C covalent bonding. Zhao also reported much weaker bonding energies for atomic, cationic, and dicationic Ca−benzene complexes as compared to other metal and metal ion−benzene complexes.[15] McKee performed theoretical studies on reactions between benzene and low work function metal atoms with ionization potentials similar to Ca[16] and suggested that reaction was initiated by transfer of an electron from the metal atom into the benzene ring.[17]

Similar attention has been directed to studies with pyridine, one of the simplest heterocyclic aromatic molecules. As the result of its simplicity, pyridine has garnered interest from surface and coordination chemists.[18] Particular interest has been focused on the reaction of pyridine with metal atoms and cations. Zero-electron-kinetic-energy (ZEKE) spectroscopy experiments coupled with DFT calculations performed by Kransnokutski and Yang[18] suggest that the pyridine−Ca^0 complex is weak due to strong repulsion between the lone pair of electrons on the pyridine N atom and the Ca 4s electrons. An understanding of metal atom and cation interactions with pyridine is also important in protein biochemistry and pharmaceutical research, because N-containing heterocycles such as nucleic acids are of biological importance.[19]

Ca has also been used extensively as an electron-selective contact in optoelectronic devices due its low work function. Unfortunately, the efficiency of devices manufactured with Ca are much lower than predicted on the basis of work function arguments alone.[20] Indeed, the reaction of postdeposited Ca with solid-state thin films of tris(8-hydroxyquinoline)aluminum (Alq_3) has been previously studied in this laboratory using Raman spectroscopy;[21] for this system, the metal forms an adduct with Alq_3 through bonding with an O atom but also causes substantial degradation of the Alq_3 into disordered

Received: February 17, 2012
Published: July 2, 2012

   dx.doi.org/10.1021/ja3016186 | J. Am. Chem. Soc. 2012, 134, 12989−12997

graphite. This study and related studies of Alq_3 with other low work function metals[22,23] demonstrate the complexity of such reactions and the difficulties in spectral interpretation attendant to such reaction chemistry in the absence of a database for solid-state organic−metal reactions. Nonetheless, this previous work did demonstrate the power of using Raman spectroscopy for elucidating many of the molecular details of these processes.

Chemical reactions in the solid state are often distinct from those of isolated molecules in that electronic properties and reaction pathways can be influenced by the proximity of neighboring molecules. In the present study, Ca atoms are reacted with thin solid-state films of benzene and pyridine. Raman spectroscopy is used for analysis of the films both before and after metal deposition. Previous studies in this laboratory[21−26] using Raman spectroscopy in UHV have demonstrated the ability of this approach to provide high molecular specificity and sensitivity to changes in molecular structure and bonding at metal−organic interfaces. Previous reports on benzene with Ag, Mg, and Al have shown formation of complexes as evidenced by the appearance of metal carbon bonds, while the more reactive pyridine has shown radical anion formation leading to new molecular entities and further degradation to amorphous carbon.[24,25]

EXPERIMENTAL SECTION

Materials. Dendritic pieces of crystalline Ca (99.98%, Alfa Aesar) were received sealed in an ampule under Ar gas and were placed in a vacuum immediately to minimize oxidation. H_2SO_4 (EM Science, ACS grade), CrO_3 (98+%, Aldrich, ACS grade), HCl (37%, Mallinckrodt, ACS grade), NH_4OH (30% NH_3, Spectrum), and HNO_3 (Mallinckrodt, ACS grade) were used as received. Water was purified (resistivity >18 MΩ, total organic content <6 ppb) using a Waters Milli-Q UV Plus System. Polycrystalline Ag stubs (7 mm thick) were cut from 12.5 mm-diam Ag rods (99.9985%, Alfa Aesar.) All other chemicals were reagent grade or better unless otherwise specified.

Ultrahigh Vacuum Chamber. The thin films used in these studies were prepared and characterized in a custom-built ultrahigh vacuum (UHV) chamber described previously.[22,23,26] Base pressures in the surface preparation chamber were maintained at $<3 \times 10^{-10}$ Torr, and working pressures were below 10^{-9} Torr. The base and working pressure in the analysis chamber were routinely maintained at 5×10^{-11} Torr.

Sample Preparation. Smooth, reflective Ag substrates[27] were used as thin film sample platforms and were mounted on a 1.5 m, closed-cycle He-cooled cryogenic translatable arm (DE-204B, Advanced Research Systems) that was routinely cooled to a base operating temperature of ca. 30 K. Temperature was controlled in these studies using a cryogenic temperature controller (Model 34, Cryo-Con) coupled to a type K (Chromel-AuFe) thermocouple located in close proximity to the Ag substrate.

After three subsequent freeze−pump−thaw cycles to remove dissolved gases, 5 monolayer (ML) thick organic films (ca. 4.9×10^{14} molecules/cm^2 of benzene and pyridine) were prepared by deposition through a glass capillary array[28] at a rate of 0.2 L/s. After acquisition of Raman spectra of the neat film, the surface was exposed to sequential 5 Å mass thickness vapor depositions (7.8×10^{14} atoms/cm^2) of Ca metal. Metal mass thickness was monitored with a liquid N_2-cooled QCM (Maxtek, Inc., model TM-400). Raman spectra were acquired after each sequential Ca deposition. These steps were repeated sequentially until a maximum of 20 Å of Ca had been deposited, and the resultant films were studied.

Instrumentation. Raman scattered photons were generated using 20−30 mW of laser power at the sample surface from a Coherent Innova 300C Ar^+ laser at 514.5 nm. The laser radiation was made p-polarized with respect to the plane of incidence using a CVI Laser Optics $\lambda/2$ Fresnel Rhomb and was incident on the surface at 60° relative to the surface normal. Scattered photons were collected at 30° with respect to the surface normal by an optical assembly including a collimating collection lens, two SuperNotch-Plus holographic notch filters (Kaiser Optical Systems) to reject Rayleigh scattering, and an f-matched focusing lens focused onto a 20 μm entrance slit of a Spex 270 M single monochromator equipped with a 1200 gr/mm grating and with a spectral bandpass of 4.6 cm^{-1} at 1000 cm^{-1}. A Roper Scientific model 400-EB 1340 × 400 pixel back-illuminated CCD camera at −90 °C was used for detection. 10 min spectral acquisition times were used.

RESULTS

Ca/Benzene. The black line in Figure 1 shows the Raman spectrum between 175−2000 cm^{-1} and 2250−3650 cm^{-1} from

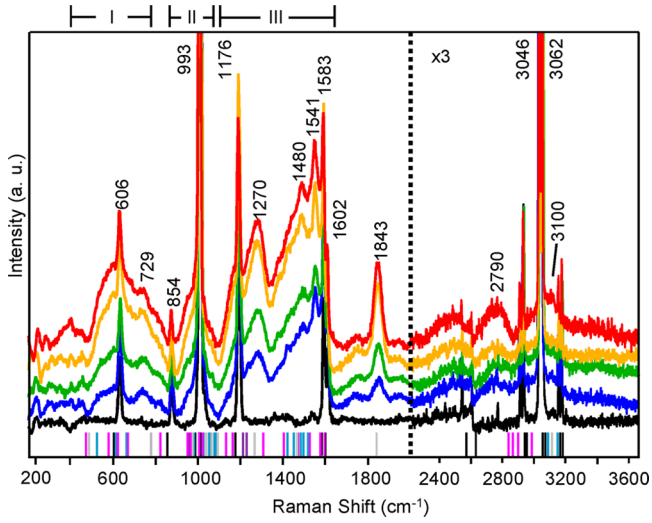

Figure 1. Raman spectra from 175−2000 and 2250−3650 cm^{-1} of 5 ML benzene thin film before (black) and after 5 Å (blue), 10 Å (green), 15 Å (yellow), and 20 Å (red) mass thickness depositions of Ca. Tick marks beneath the spectra identify known frequencies for benzene (black), phenyl radical anion (pink), phenyl radical (aqua), benzyne (gray), and CaH/CaH_2 (purple). Frequency regions labeled as I, II, and III are discussed in the text.

an amorphous,[29] 5 ML solid-state benzene film. The blue, green, yellow, and red lines show the Raman spectra of the film after vapor deposition of 5, 10, 15, and 20 Å mass thicknesses of Ca, respectively. Eight sharp bands assigned to vibrational modes of benzene can be seen in these spectra; these are tabulated and assigned in Table S1 of the Supporting Information. Seven in-plane (ip) modes (ν_6 at 606 cm^{-1}, ν_1 at 993 cm^{-1}, ν_9 at 1176 cm^{-1}, ν_{8a} and ν_{8b} at 1583 and 1602 cm^{-1}, respectively, ν_7 at 3046 cm^{-1}, and ν_2 at 3062 cm^{-1}) and one out-of-plane mode (oop) (ν_{10} at 854 cm^{-1})[30,31] can be distinguished above the background.

Upon deposition of Ca, spectral changes indicate reaction chemistry between Ca and the benzene film. New features are observed in the spectra that cannot be assigned to any benzene mode.[30,31] These new features appear as three broad envelopes between 450−800 cm^{-1} (denoted as frequency region I), 900−1050 cm^{-1} (frequency region II), and 1075−1650 cm^{-1} (frequency region III). In addition, several new discrete bands are observed at 729, 1270, 1480, 1541, and 1843 cm^{-1}. Spectroscopic changes in the higher frequency region (2500−3300 cm^{-1}) are more subtle: a weak, broad band centered at ca. 2800 cm^{-1} and a broadening of the ν(C−H) bands above 3000 cm^{-1}. No spectral evidence for Ca−benzene adduct formation,

dx.doi.org/10.1021/ja3016186 | J. Am. Chem. Soc. 2012, 134, 12989−12997

which would be apparent as a band at ca. 170 cm^{-1} from the ν(Ca−C) mode,[32] is observed.

Spectral assignments are facilitated by an understanding of the known reaction chemistry between Ca and benzene in various environments. Vapor-phase Ca atoms and co-condensed benzene have been shown to form aryl calcium hydrides by insertion of Ca^+ into an aryl C−H bond.[33,34] The pathway by which this product is formed involves electron transfer from Ca to the phenyl radical anion, followed by attack of the resulting Ca^+ on an electron-rich site.[33,34] Matrix isolation ESR studies of Ca atoms in the presence of benzene have confirmed the presence of the phenyl radical anion.[35] If the phenyl radical undergoes a second C−H bond scission, benzyne is formed.[36] Zhang et al.[37] have studied the three possible diradical arrangements in benzyne using time-of-flight photoionizaton mass spectrometry (TOF-PIMS), matrix isolation IR spectroscopy, and chemical ionization-mass spectrometry (CIMS) and have concluded that the *o*-benzyne isomer is the most stable.

The spectra in Figure 1 can be interpreted on the basis of this previously proposed reaction chemistry initiated by metal-to-organic electron transfer. This interpretation is further facilitated by previous spectral studies of the phenyl radical anion, the neutral phenyl radical, and benzyne that have been reported in the literature. Lipinski and co-workers[5] reported Raman spectra of the phenyl radical in an Ar matrix at 7 K. Huang and co-workers[4] used both ab initio and DFT calculations to predict the vibrational spectra for benzene and its corresponding cation and anion radicals. *o*-Benzyne has been isolated in an Ar matrix and studied using IR spectroscopy by Radziszewski and co-workers,[7] and its vibrational spectrum has been theoretically calculated by Liu et al.[6] The frequencies from this previous work match well with the new bands observed in Figure 1. The frequencies for the vibrational bands for the phenyl radical anion, the phenyl radical, and benzyne from this previous work are shown as tick marks colored by species beneath the spectra in Figure 1, with the benzene bands in black, the phenyl radical anion bands in pink, phenyl radical bands in aqua, the benzyne bands in gray, and those for CaH/CaH_2 in purple. Assignments and frequencies for these tick marks are included in Table S1 of the Supporting Information.

A proposed reaction scheme is illustrated in Figure 2. Mitsui et al. have documented an increase in the electron affinity of

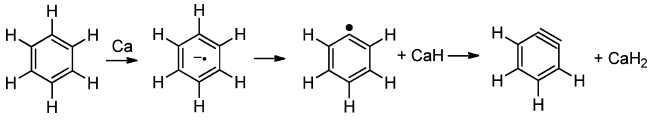

Figure 2. Proposed reaction scheme for benzene with atomic Ca involving stepwise formation of the phenyl radical anion, phenyl radical, benzyne, CaH, and CaH_2.[3−7]

benzene upon condensation into clusters from −1.15 eV[38] for isolated molecules to <0.3 eV[39] for clusters, the latter of which was determined from measured vertical dissociation energies. A parallel can be drawn between the influence of clustering on electron affinity and the condensed thin films used here. This increase in electron affinity makes charge transfer from Ca to benzene favorable, resulting in the formation of a phenyl radical anion species, which is predicted to exhibit 23 vibrational bands in the frequency regions studied here.[4] Upon deposition of Ca, frequency region I exhibits broad new spectral features that are consistent with six of these bands: ν_{10} at 578 cm^{-1}, ν_{27} at 617 cm^{-1}, ν_{17} at 661 cm^{-1}, ν_{16} at 705 cm^{-1}, ν_{15} at 817 cm^{-1}, and ν_{12} at 838 cm^{-1}.[4] Four additional phenyl radical anion bands are predicted in spectral region II: ν_9, ν_8, ν_{26}, and ν_7 at 924, 980, 1009, and 1027 cm^{-1}, respectively. The phenyl radical anion has eight vibrational bands throughout frequency region III that overlap with the broad new bands observed after reaction with Ca. These bands include those at 1129, 1165, 1225, 1310, 1396, 1414, 1525, and 1526 cm^{-1}, assigned to the ν_{25}, ν_6, ν_{24}, ν_{23}, ν_{22}, ν_5, ν_4, and ν_{21} modes, respectively. Five vibrational bands are also predicted between 2850 and 3030 cm^{-1} that match well with new spectral features observed here, including the ν_{20}, ν_3, ν_2, ν_{19}, and ν_1 modes at 2858, 2860, 2936, 2940, and 3031 cm^{-1}, respectively. The new broad band centered near 2800 cm^{-1} in the spectra after reaction with Ca is assigned to overtones of the new broad band observed in region III.

The phenyl radical is formed upon loss of a hydride from the phenyl radical anion species, and has 22 vibrational modes predicted across the frequency regions investigated here.[5] Five phenyl radical bands are predicted in frequency region I at 582, 603, 646, 706, and 781 cm^{-1}, assigned to the ν_{27}, ν_{10}, ν_{17}, ν_{16}, and ν_{12} modes. The ν_{15} mode overlaps the ν_{10} neat benzene mode at 857 cm^{-1}. Six vibrational bands are predicted throughout region II from the ν_{11}, ν_9, ν_{14}, ν_8, ν_7, and ν_{26} modes at 945, 973, 990, 998, 1028, and 1047 cm^{-1}, respectively. Spectral region III is predicted to contain five phenyl radical bands at 1151, 1159, 1281, 1310, and 1497 cm^{-1}, assigned to ν_6, ν_{25}, ν_{24}, ν_{23}, and ν_4 modes, respectively. There are also five bands predicted between 3080 and 3120 cm^{-1}, including the ν_3, ν_{20}, ν_2, ν_{19}, and ν_1 modes at 3083, 3089, 3102, 3104, and 3117 cm^{-1}, respectively. These bands may contribute to the band centered near 3100 cm^{-1} in Figure 1.

Loss of an additional hydrogen from the phenyl radical species results in the benzyne molecule, which is formally a diradical species. On the basis of previous DFT calculations and matrix isolation IR spectroscopy, benzyne is predicted to have 16 vibrational bands in the frequency regions studied here.[6,7] In spectral region I, two bands assigned to $\delta(C-C-C)_{ip}$ modes are predicted at 472 and 589 cm^{-1}. A $\delta(C-H)_{ip}$ band is predicted at 838 cm^{-1}. Spectral region II has three benzyne modes: the $\nu(C-H)_{ring}$ mode at 982 cm^{-1}, the ν(C−H) mode at 1039 cm^{-1}, and the $\delta(C-H)_{oop}$ mode at 1094 cm^{-1}. Five vibrational modes are predicted in spectral region III, including four $\nu(C-H)_{ip}$ bands at 1271, 1307, 1394, and 1415 cm^{-1} and one ν(C−C) band at 1451 cm^{-1}. The discrete band observed at 1846 cm^{-1}, assigned to the ν(C≡C) mode of benzyne,[7] is the most definitive signature for benzyne in the reaction products in these films, as this region of the vibrational spectrum is normally silent. This vibrational band at 1860 cm^{-1} was first assigned to a ν(C≡C) mode by Leopold et al.[40] Finally, four benzyne ν(C−H) modes are predicted between 3050 and 3100 cm^{-1} that may contribute to the observed broad band centered at 3100 cm^{-1}.

As is shown in Figure 2, loss of a hydride to form the neutral phenyl radical species results in the formation of CaH; loss of a subsequent hydrogen atom produces the benzyne diradical molecule and CaH_2. Wang and Andrews[3] have reported the matrix isolated IR spectra along with the corresponding DFT calculated spectra of CaH_2 and CaH; these molecules exhibit multiple bands between 1185 and 1394 cm^{-1}. $\nu(CaH_2)$ bands should appear at 1185, 1194, and 1215 cm^{-1}, and ν(Ca−H) bands should be observed at 1250, 1290, and 1394 cm^{-1}; these frequencies are denoted with purple tick marks in Figure 1.

dx.doi.org/10.1021/ja3016186 | J. Am. Chem. Soc. 2012, 134, 12989−12997

While many of these modes are likely subsumed by the broad spectral features observed in these spectra, observation of a band at 1270 cm^{-1} is a good indication of the presence of this metal hydride.

Ca/Pyridine. The black line in Figure 3 shows the Raman spectrum of a similar amorphous,[41] solid-state pyridine film.

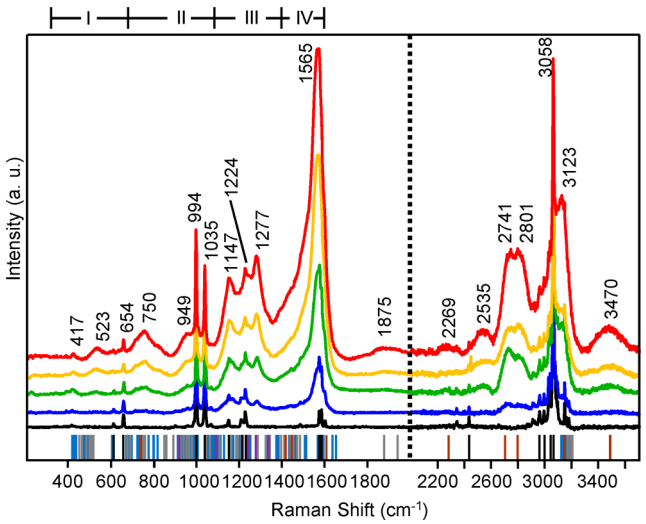

Figure 3. Raman spectra from 175−2000 cm^{-1} and 2050−3650 cm^{-1} of 5 ML pyridine thin film before (black) and after 5 Å (blue), 10 Å (green), 15 Å (yellow), and 20 Å (red) mass thickness depositions of Ca. Tick marks beneath the spectra identify known frequencies for pyridine (black), pyridyl radical (aqua), pyridyne (gray), ring-opening products (brown), and CaH/CaH_2 (purple). Frequency regions labeled as I, II, III, and IV are discussed in the text.

The blue, green, yellow, and red lines show the Raman spectra of the film after vapor deposition of 5, 10, 15, and 20 Å mass thickness of Ca, respectively. Fifteen Raman-active bands can be distinguished in the spectrum of the pristine pyridine film: nine in-plane modes (ν_1, ν_{6a}, ν_{6b}, ν_{8a}, ν_{8b}, ν_{9a}, ν_{12}, ν_{14}, ν_{15}), one out-of-plane mode (ν_{16b}), one combination band ($\nu_1 + \nu_{6a}$), and four ν(C−H) modes.[42] Assignments for these bands are found in Table S3 of the Supporting Information. The most intense of these bands is the ν_1 symmetric ring breathing mode at 994 cm^{-1}.

Several new Raman bands are observed after deposition of Ca, indicating reaction chemistry between Ca and pyridine. Although some of the features in these spectra can be assigned to unreacted pyridine,[42] the new spectral features are indicative of reaction product formation. Three very broad features can be seen at 523, 750, and 949 cm^{-1} upon deposition of Ca. New bands also grow in at 1147 and 1277 cm^{-1} that are superimposed on a broad background ranging from ca. 1100 to 1350 cm^{-1}. The product spectra are dominated by a broad asymmetric band that spans the range from ca. 1380 to 1600 cm^{-1}. Additionally, a new weak, broad band is observed at 1875 cm^{-1}, and six new broad bands in the ν(C−H) region are observed at 2269, 2535, 2741, 2801, 3123, and 3470 cm^{-1}. In general, these new bands are from reaction products between Ca and pyridine, which are of greater relative intensity than observed after reaction of Ca with benzene, indicating greater reactivity of pyridine if the assumption of approximately comparable Raman scattering cross sections is valid. To facilitate discussion of these data, new spectral features are distinguished in four distinct frequency regions. Region I from 400−600 cm^{-1} encompasses the new broad band observed at 520 cm^{-1}. Region II from 600−1050 cm^{-1} encompasses the two broad spectral features at 750 and 950 cm^{-1}. The region between 1050 and 1400 cm^{-1} is designated as region III, and the region between 1400 and 1600 cm^{-1} is denoted as region IV.

Before the new features in these spectra are assigned, consideration of the possible reaction products of pyridine with Ca is useful. As shown previously for benzene clusters, the electron affinity of pyridine changes from −0.62 eV[43] for the free molecule to 1.02 eV[44] for pyridine clusters, based on the electron binding affinity measured by photoelectron spectroscopy. This increase of electron affinity makes favorable a Ca-to-pyridine electron transfer. This electron transfer is consistent with what has been reported by Wang and co-workers on the basis of reflection time-of-flight mass spectrometry studies.[45] ESR studies performed by Kasai and McLeod[46] demonstrated formation of the pyridyl radical anion via dissociative electron capture from Na in an argon matrix. Shvartsburg suggested that the pyridyl radical anion can then undergo dissociative transfer of a hydride to produce the pyridyl radical and the metal hydride.[47] The *o*-, *m*-, and *p*-pyridyl radical species are possible, and all have been observed previously in pulse radiolysis studies of liquid pyridine,[48] dissociative electron capture studies using ESR,[46] and neutralization−reionization mass spectrometry.[49] Additionally, vibrational frequencies for all three radicals have been calculated by LaVerne et al.[50] After formation, these radicals may also undergo ring-opening reactions to form degradation products as have been observed in ESI-MS/MS,[47] IR spectroscopy,[51] and ESR[46] experiments, as well as predicted in many theoretical calculations.[1,52−55]

The loss of a hydrogen from the pyridyl radical species results in pyridyl diradical (pyridyne) formation, which has been observed in the previously mentioned ESR studies by Kasai and McLeod.[46] 3,4-Pyridyne was first directly observed by Nam and Leroi[56] using matrix isolation IR spectroscopy of the reaction of 3,4-pyridine dicarboxcylic acid by UV photolysis. 3,5-Pyridyne has also been produced by Winkler et al.[51] with vacuum pyrolysis of 3,5-diiodopyridine and characterized by matrix isolation IR. It has been suggested that pyridyne is unstable,[51,56] and many calculations have been reported on the degradation pathways of both 3,4- and 3,5-pyridyne.[1,2,52−55] DFT calculations by Cheng et al. have also suggested a series of degradation products arising from ring-opening of the *o*-, *m*-, and *p*-pyridyl radical. In fact, the energies of these products are slightly lower than those of both 2,3- and 3,4-pyridyne. Because of this fact, production of these acyclic species should be preferred relative to pyridyne production.

Figure 4 shows a proposed reaction pathway for solid-state pyridine films with vapor-deposited Ca derived from this collective previous work; this pathway fully rationalizes the spectral data presented here. Detailed spectral assignments and frequencies for each species compiled from the experimental and theoretical reports cited above are provided in Table S3 of the Supporting Information. Color-coded tick marks for all of the modes either observed or predicted for each of the species are included beneath the spectra in Figure 3. Black tick marks indicate unreacted pyridine modes, pyridyl radical modes are denoted in aqua, modes belonging to the pyridyne species are marked in gray, brown tick marks are used to show modes that belong to degradation products arising from ring-opening, and CaH/CaH_2 modes are denoted in purple.

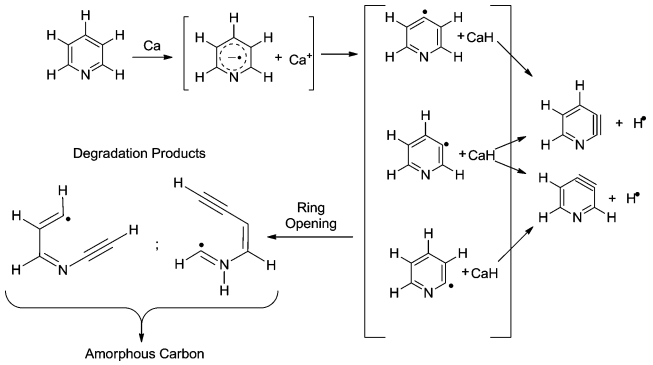

Figure 4. Proposed reaction scheme for pyridine with atomic Ca yielding the pyridyl radical species, the pyridynes, and ring-opening degradation products.[1−3]

The most distinct feature in region I is the small broad band centered near 523 cm^{-1} that can be attributed to the out-of-plane C−H bending and in-plane C−C−C and C−H bending modes of several ring-opening products calculated by Cheng et al.[1,52,53] The other spectral feature in this region, the band at 417 cm^{-1}, is also seen in the pristine pyridine film spectrum and can be assigned to an overlap of pyridine out-of-plane bending modes and *o*- and *m*-pyridyl radical bending modes[50] at 417 and 414 cm^{-1}, respectively, as well as the out-of-plane molecular bending mode of 2,3-pyridyne at 411 cm^{-1}.[52]

Frequency region II covers the range from 600 to 1050 cm^{-1}. The new broad band centered at ca. 750 cm^{-1} most likely consists of bands from multiple species including those from pyridine, *o*-, *m*-, and *p*-pyridyl radical, 2,3- and 3,4-pyridyne, as well as many bands predicted for ring-opening degradation products. The first of these, unreacted pyridine, has two bands within this envelope, the out-of-plane C−H bending at 703 cm^{-1} and the out-of-plane ring twist at 747 cm^{-1}.[42] The *o*-, *m*-, and *p*-pyridyl radicals also have frequencies for these two modes at 700 and 739 cm^{-1}, 700 and 739 cm^{-1}, and 697 and 754 cm^{-1}, respectively.[50] A third C−H bending mode for *p*-pyridyl radical at 810 cm^{-1} is also contained in this band.[50] Four additional bands, two each for 2,3-pyridyne, the in-plane molecular bend (712 cm^{-1}) and an out-of-plane C−H bend (814 cm^{-1}), and 3,4-pyridyne, the out-of-plane C−H bending (818 cm^{-1}) and δ(N−C−C) (848 cm^{-1}), also fall within this envelope.[52] Finally, several bending modes for degradation products are also expected to contribute to this band.[1,52,53]

Also within region II is the broad band centered at 949 cm^{-1}. As with the broad band at 750 cm^{-1}, several modes from pyridine, all three pyridyl radicals,[50] and both pyridynes[52] contribute to this band. Out-of-plane C−H bending vibrations for pyridine[42] at 941 cm^{-1}, *o*-pyridyl at 939 cm^{-1}, *m*-pyridyl at 925 cm^{-1}, *p*-pyridyl at 915 cm^{-1}, and 3,4-pyridyne at 915 and 944 cm^{-1} all contribute to this band. The three pyridyl radicals also have $\nu(C-H)_{ring}$ modes within this envelope at 950 (*o*-), 972 and 973 cm^{-1} (*m*-), and 961 and 963 cm^{-1} (*p*-).[50] Additionally, two skeletal bending modes of 2,3-pyridyne can be assigned at 926 and 975 cm^{-1}.[52]

Three additional bands in region II can be assigned almost exclusively to modes of unreacted pyridine at 654, 994, and 1035 cm^{-1}.[42] While the bands at 994 and 1035 cm^{-1} are solely attributed to $\nu(C-H)_{ring}$ and δ(ring) modes, respectively, the band at 654 cm^{-1} is assigned to in-plane ring deformations for pyridine and all three pyridyl radicals, as they all occur at about the same frequency.[42,50]

Region III between 1050 and 1400 cm^{-1} is dominated by a large broad band centered near 1200 cm^{-1} on which three sharper bands are superimposed. This broad spectral feature is likely the D-band of amorphous carbon.[57] The first of the discrete bands at 1147 cm^{-1} can be attributed primarily to the in-plane C−H deformations of pyridine (1146 cm^{-1}),[42] *o*- and *m*-pyridyl radical (1150 and 1147 cm^{-1}),[50] 3,4-pyridyne (1169 cm^{-1}),[52] and the $\nu(Ca-H_2)$ of calcium hydride (1185 cm^{-1}). The second band at 1224 cm^{-1} can also be attributed to the in-plane C−H deformations of pyridine (1227 cm^{-1}), *o*-pyridyl (1228 cm^{-1}), *m*-pyridyl (1222 cm^{-1}), *p*-pyridyl (1217 and 1219 cm^{-1}) 3,4-pyridyne (1247 cm^{-1}),[52] as well as the $\nu(Ca-H_2)$ and ν(Ca−H) of the calcium hydrides at 1215 and 1250 cm^{-1}, respectively. The third and final band of this region can be attributed to the in-plane C−H deformations of *m*- and *p*-pyridyl[50] and 3,4-pyridyne[52] at 1294, 1291, and 1292 cm^{-1}, respectively, as well as another ν(Ca−H) mode at 1290 cm^{-1}.

Region IV is comprised predominantly of a broad asymmetric band that fills the entire spectral region between 1400−1600 cm^{-1}; this is characteristic of the G band of amorphous carbon.[57] Also in this region are the $\nu(ring)_{ip}$ modes of pyridine (1574 and 1581 cm^{-1})[42] and all three pyridyl radicals,[50] *o*- (1389 and 1464 cm^{-1}), *m*- (1564 cm^{-1}), and *p*- (1436, 1491 cm^{-1}), which comprise the intense band at 1565 cm^{-1}. This band also encompasses the in-plane C−H deformations for pyridine (1437 and 1410 cm^{-1}),[42] *o*-pyridyl (1389 and 1464 cm^{-1}),[50] *m*-pyridyl (1434 and 1495 cm^{-1}),[50] *p*-pyridyl (1436 and 1491 cm^{-1}),[50] 2,3-pyridyne (1410 cm^{-1}),[52] and 3,4-pyridyne (1457 cm^{-1}).[52] The in-plane H−C−C−H deformations for 2,3-pyridyne at 1445 and 1474 cm^{-1} additionally contribute to this region.[52]

One other weak and broad but distinct band in the frequency region below 2000 cm^{-1} is observed at 1875 cm^{-1}. This band is assigned to the $\nu(C{\equiv}C)_{ip}$ modes of 2,3-pyridyne (1863 cm^{-1}) and 3,4-pyridyne (1871 cm^{-1}).[52] In contrast to the relatively large intensity of this band for the benzyne product of the reaction of Ca with benzene as discussed above, very little pyridyne is present within these films. A second significant difference between these two aromatic systems is the prominent spectral signature of amorphous carbon in the spectra from the Ca/pyridine reaction but its complete absence in the spectra from the Ca/benzene reaction.

Further evidence for degradation of the pyridine film via radical ring-opening can be found in the high frequency region (>2200 cm^{-1}). Three broad bands at 2269, 2535, and 3470 cm^{-1} are indicative of acyclic alkynes and nitriles; these three bands can be assigned as $\nu(C{\equiv}C)$, $\nu(C{\equiv}N)$, and $\nu({\equiv}C-H)$ modes, respectively.[1,52,53] These functionalities could only exist by ring-opening processes during degradation. Representative degradation products can be seen in Figure S1 of the Supporting Information with their frequencies tabulated in Table S4.

Two additional broad bands are observed at 2741 and 2801 cm^{-1}; these are most likely attributable to the 2D modes of amorphous carbon. Interestingly, evidence for a 2D mode is also observed in the spectral data for benzene/Ca (Figure 1) but is much weaker. As noted above, overtones of the intense bands at ca. 1400 cm^{-1} are also likely to contribute to this band in the benzene system. Finally, the broad shoulder centered at 3123 cm^{-1} on the high frequency side of the pyridine C−H stretching band at 3058 cm^{-1} is attributed to ν(H−C=C−H) modes of degradation products as shown in Figure 4.[1,52,53]

dx.doi.org/10.1021/ja3016186 | J. Am. Chem. Soc. 2012, 134, 12989−12997

Ca/Pyridine-d_5. Reactions between Ca and thin, solid-state films of the perdeuterated forms of benzene and pyridine were investigated for additional insight into the proposed reaction pathways. The black line in Figure 5 shows the Raman spectrum of a 5 ML solid-state film of pyridine-d_5. The blue, green, yellow, and red lines show the Raman spectra of the film after deposition of 5, 10, 15, and 20 Å mass thicknesses of Ca, respectively. The vibrational bands for the pristine pyridine-d_5 film are observed at frequencies identical to those previously reported by Kozhevina et al.[58] These are tabulated in Table S6 of the Supporting Information.

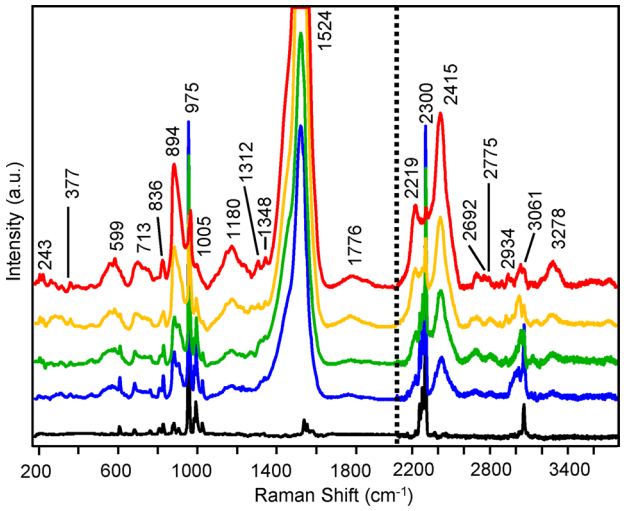

Figure 5. Raman spectra from 175−2000 cm^{-1} and 2050−3650 cm^{-1} of 5 ML pyridine-d_5 thin film before (black) and after 5 Å (blue), 10 Å (green), 15 Å (yellow), and 20 Å (red) mass thickness depositions of Ca.

Although the literature contains very little information about pyridine-d_5 or its reduction products (i.e., pyridiyl-d_5 radical anion, pyridyl-d_4 radical, pyridyl-d_4 ring-opening products), some qualitative information can be gained from the spectra in Figure 5. Upon deposition of Ca, reaction chemistry occurs that parallels that of the pyridine−Ca system as described above. A broad, asymmetric band between 1300 and 1600 cm^{-1} appears due to the formation of amorphous carbon. In addition, new broad bands appear near 599, 713, and 1180 cm^{-1}. These are attributed to the $\delta(\text{C}-\text{D})_{\text{oop}}$, $\nu(\text{C}-\text{D})_{\text{ring}}$, and $\delta(\text{C}-\text{D})_{\text{ip}}$ modes, respectively, of *o,m,p*-pyridyl-d_4 radicals, as well as both possible pyridyne-d_3 species, based on their observation at frequencies lower than those reported above for the pyridyne species at 750, 950, and 1250 cm^{-1}. Moreover, the 1875 cm^{-1} $\nu(\text{C}\equiv\text{C})$ band from the pyridyne diradical species is observed at the lower frequency of 1776 cm^{-1} for the pyridyne-d_3 species. Additionally, the lower frequency bands between 200 and 400 cm^{-1} are consistent with a pyridyl-d_4 radical species. One particularly useful new band appears near 900 cm^{-1} upon Ca deposition. This band is tentatively assigned to the ν(Ca−D) mode based on its shift to lower frequency by ca. 250 cm^{-1} from the ν(Ca−H) mode at 1277 cm^{-1} for the Ca/pyridine system. Although there is no literature precedent for this assignment, the shift matches closely to what would be predicted from a simple Hooke's law analysis for the heavier isotope.

Bands in the high frequency region are also characterized by similar shifts to lower frequency; most notably, the ν(C−D) mode for the pyridyl-d_4 radicals is observed at 2415 cm^{-1} as compared to its position at 3123 cm^{-1} for pyridyl radicals. The band at 3278 cm^{-1} is assigned to the $\nu(\equiv\text{C}-\text{D})$ mode of pyridyl-d_4 radical degradation products. This is shifted down by ca. 200 cm^{-1} from the analogous band at 3470 cm^{-1} for pyridyl radical degradation products. The other two bands expected for the $\nu(\text{C}\equiv\text{C})$ and $\nu(\text{C}\equiv\text{N})$ modes from degradation products for the pyridine-d_5 system near 2269 and 2535 cm^{-1}, respectively, cannot be distinguished due to significant spectral overlap with the ν(C−D) modes. Additional spectral complexity arises from the presence of hydrogenated pyridine (and its reaction products) in the system as indicated by the presence of its ν(C−H) bands at ca. 3000 cm^{-1}.

Ca/Benzene-d_6. The black line in Figure 6 shows the Raman spectrum from a 5 ML solid-state benzene-d_6 film. The blue, green, yellow, and red lines show the Raman spectra of the film post deposition of 5, 10, 15, and 20 Å mass thickness of Ca, respectively. The bands for the pristine film match closely the frequencies reported previously for a 200 ML benzene-d_6 film on Ag reported by Moskovits and DiLella;[30] their assignments are given in Table S7 of the Supporting Information.

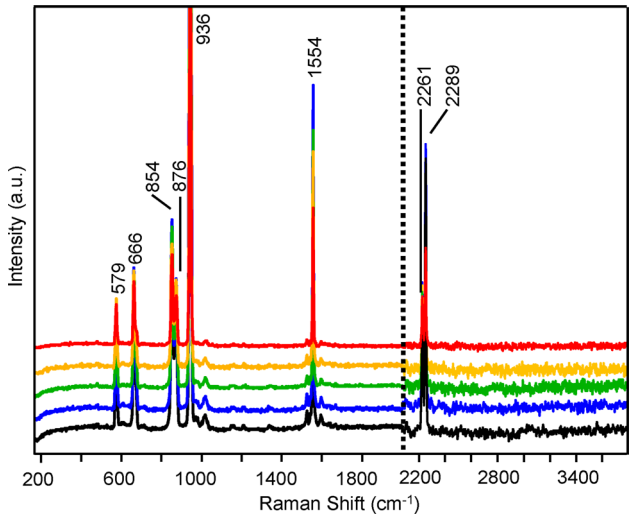

Figure 6. Raman spectra from 175−2000 cm^{-1} and 2050−3650 cm^{-1} of 5 ML benzene-d_6 thin film before (black) and after 5 Å (blue), 10 Å (green), 15 Å (yellow), and 20 Å (red) mass thickness depositions of Ca.

Surprisingly, upon deposition of Ca onto the benzene-d_6 film, no new bands are observed, indicating that no reaction chemistry analogous to that for the Ca/benzene system occurs. The only observable spectral change is a significant reduction in signal intensity for all benzene-d_6 modes, decreasing to ca. 50% of the initial intensity after deposition of 20 Å Ca. This reduction in signal intensity is attributed to formation of an increasingly opaque metallic Ca overlayer, which limits both the number of exciting photons that reach the organic film and the number of Raman scattered photons that are collected.

Figure 7 shows plots of the normalized intensity ratio of a reaction product band for each of these molecular systems relative to a band attributable to the remaining unreacted molecules as a function of Ca mass thickness. Bands used for the unreacted molecules include the distinct and intense ν(C−H) or ν(C−D) ring modes (ν_1) for benzene (993 cm^{-1}), benzene-d_6 (936 cm^{-1}), pyridine (994 cm^{-1}), and pyridine-d_5

dx.doi.org/10.1021/ja3016186 | J. Am. Chem. Soc. 2012, 134, 12989−12997

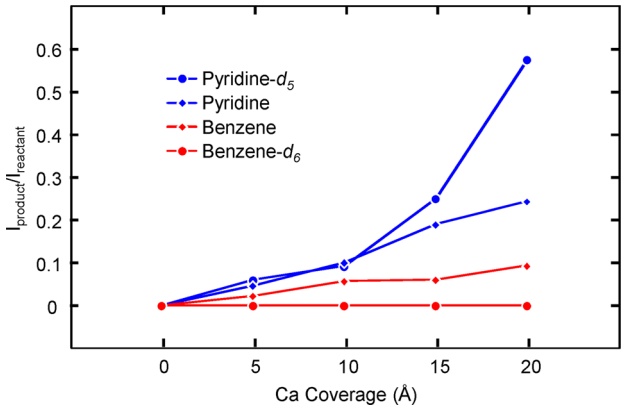

Figure 7. Ratio of Raman band intensities for reaction products relative to the ν_1 ring mode for unreacted molecules after deposition of varying mass thicknesses of Ca. Reaction product band frequency used for benzene, 1843 cm^{-1}; pyridine, 750 cm^{-1}; and pyridine-d_5, 599 cm^{-1}. See text for discussion of intensity ratio for benzene-d_6.

(975 cm^{-1}). For pyridine, the reaction product $\delta(ring)_{oop}/\delta(C-H)_{oop}$ band at 750 cm^{-1} was chosen for this plot due to its spectral isolation and sensitivity to reaction with Ca. The corresponding $\delta(ring)_{oop}/\delta(C-D)_{oop}$ band at 599 cm^{-1} was used for pyridine-d_5. For benzene, the very distinct and isolated benzyne $\nu(C\equiv C)$ mode at 1843 cm^{-1} was chosen for this plot; however, due to the lack of reactivity of Ca with benzene-d_6, this normalized intensity ratio remains at zero for any frequency except those associated with the pristine benzene-d_6 film.

DISCUSSION

Previous studies of Ca and benzene in the gas and liquid phases and in matrix isolation studies have revealed the presence of the phenyl radical and phenyl radical anion species.[33−35,59,60] Further reduction of the radical species leads to the formation of benzyne, formally a benzene diradical.[36] The mechanism used to explain this reaction, as shown in Figure 2, is similar to the pyrolysis mechanism of benzene first proposed by Bauer and Aten.[61] These same products have also been observed in studies of the combustion of gasoline, which may contain up to 20−30% of small aromatic molecules including benzene.[62] Similarly, the reaction of pyridine with Ca results in the formation of pyridyl radical, pyridyne, as well as further decomposition products due to ring-opening.[1,47,51−53]

It is apparent from the comparison in Figure 7 that Ca is considerably more reactive with pyridine than with benzene. Consideration of previous theoretical studies of the gas-phase degradation energetics for both molecules by the proposed pathways is useful in rationalizing the extent of these reactions. It is worth noting, however, that on the basis of the spectral evidence as detailed above, one concludes that these reactions in solid-state films are considerably more favorable than those predicted for these molecules in the gas phase due to the stabilizing effects of solid-state solvation in the thin films.

In the case of benzene, Davico[63] calculated the heat of formation of the phenyl radical species from benzene at 0 K to be 84.3 ± 0.6 kcal mol^{-1}. Calculations by Madden[64] and Zhang[37] on decomposition of the phenyl radical suggest a heat of formation for *o*-benzyne of 76 kcal/mol, ca. 22 kcal/mol less than for formation of the corresponding ring-opening products C_4H_3 and C_2H_2. Deng[65] reported that the decomposition of benzyne to C_2H_2 and C_4H_3 has an even larger energy barrier of 88.6 kcal/mol, in good agreement with the work of Moskaleva[62] that suggested that isomerization of *o*-benzyne to *p*- and *m*-benzyne is more favorable than formation of ring-opening products. These previous calculations are in good agreement with the solid-state spectra reported here, which document that the decomposition of benzene is induced by electron transfer from Ca to form the phenyl radical and benzyne, with no evidence for ring-opening.

Although to our knowledge, no studies have been undertaken to define the energetics of the reaction of pyridine to the pyridyl radical, calculations by Liu[54] suggest that degradation of the pyridyl radical to pyridyne is energetically accessible. The transition to 3,4-pyridyne and 2,3-pyridyne from *o*-pyridyl requires 80.9 and 86.6 kcal/mol, respectively.[54] However, a more energetically favorable pathway by ring-opening is accessible, requiring between 40 and 80 kcal/mol,[1,52−54] although complete degradation of pyridine to species such as C_2H_2 and HCN is less likely, with barriers greater than 110 kcal/mol.[54] The results of these calculations further substantiate the conclusions drawn here that the spectral evidence in the Ca/pyridine system suggests an abundance of ring-opening products with the possibility of small amounts of pyridyne formed and the absence of complete degradation to very simple molecules such as C_2H_2 and HCN.

The spectra for the reaction of Ca with pyridine-d_5 are entirely consistent with the reaction pathway proposed for pyridine. This similarity further supports the assertion of metal-to-organic electron transfer as the first step in these reactions resulting in the formation of radical anions leading both to degradation to amorphous carbon and ring-open products as well as to formation of the diradical pyridyne species. Although one might expect the degree of reactivity to be similar for thin films of the hydrogenated and perdeuterated isotopologues of these simple organic systems, the plots in Figure 7 suggest that pyridine-d_5 is more reactive than pyridine by a factor of at least 2.

In contrast, benzene-d_6 exhibits essentially no reactivity with Ca, whereas the corresponding benzene films demonstrably react with deposited Ca. At present, we have no concrete explanation for this striking reactivity difference. Although little previous research has been undertaken to elucidate the reactivity of the phenyl-d_6 radical anion, Stevenson and co-workers have reported the results of gas[66]- and solution[67]-phase ESR studies of the reduction of mixtures of benzene and benzene-d_6 with potassium metal that document greater reactivity of the hydrogenated phenyl radical anion over the phenyl-d_6 radical anion by more than a factor of 2. These researchers attributed this difference in reactivity to the slightly lower (0.5 kcal/mol) electron affinity of benzene-d_6 relative to benzene. This slight difference in electron affinity seems insufficient to rationalize the pronounced difference in reactivity of the benzene-d_6 and benzene thin films studied here, suggesting the dominance of additional unidentified factors. Although a full description of these factors is desirable, attaining this understanding will require additional experiments and methods well beyond the scope of this study.

In total, this study expands the existing knowledge base of simple aryl−Ca reactions to include results on these solid-state organics that may have direct implications for astrochemical and optoelectronic systems. Molecules such as benzene, phenyl radical, benzyne, C_4H_3, and C_2H_2 are proposed intermediates in the formation of PAHs in protoplanetary nebula,[68] and Weaver identified the need to study benzene and its derivatives to obtain a full understanding of the PAH formation mechanism.[8]

dx.doi.org/10.1021/ja3016186 | J. Am. Chem. Soc. 2012, 134, 12989−12997

Although the present study involves decomposition of benzene into the phenyl radical and benzyne via electron injection into the parent molecule, it demonstrates the relationship of the three molecules discussed herein. Conversely, Fries and Steele[11] have proposed that graphite whiskers (GWs) form in the vicinity of Ca inclusions in meteorites that are in close proximity to a sun via condensation reactions of simple organic molecules. These researchers further note that GWs have been produced in the lab at high temperatures, suggesting that Ca degrades simple organic molecules into their dehydrogenated counterparts[11] that eventually condense into graphitic structures.[69] It is important to note that the studies in this report were carried out near 30 K, and while no graphite may have been observed, neither long-term kinetic nor thermodynamic studies were performed. Thermodynamic studies for these molecules are difficult to perform at UHV pressures due to the relatively low melting point of these organics.

In optoelectronic devices, charge injection/collection between a metal electrode and an organic layer is critical for device efficiency,[70] and much effort has been expended to make the energy barrier between the two materials as small as possible through strategies such as chemical modification of the electrode[71] or the addition of a blocking layer between the organic and the metal,[72−77] although the basis of the enhanced performance is still under debate.[78−81] The presence of reaction products between the organic layer and the metal may significantly alter interface energetics, making it impossible to predict the injection barrier present at the interface.

Indeed, in the simple cases of benzene and pyridine, which are common chemical moieties found in many optoelectronic organic materials, energy changes occur upon degradation. In benzene, the $\pi\rightarrow\pi^*$ transition, which represents the HOMO−LUMO energy level gap, is 6.89 eV.[82] This gap decreases to 5.28 eV for the phenyl radical,[83] and 3.26 eV in *o*-benzyne.[84] Similarly, the $\pi\rightarrow\pi^*$ transition in pyridine is 6.38 eV, which decreases to 5.43 eV upon the formation of the Ca^+−pyridine complex.[85] Because of the loss of an electron, the HOMO of the pyridyl radical becomes a SOMO (singularly occupied molecular orbital), which in turn causes the gap between the SOMO and the LUMO to decrease to a value as low as 2.5 eV for all three radicals.[86] These significant energy changes due to reaction chemistry at the metal−organic interface may account for differences in the theoretically and experimentally obtainable performance in these devices.

CONCLUSIONS

We report here the solid-state reaction chemistry of thin benzene and pyridine films with postdeposited Ca. This reaction chemistry is initiated by metal-to-organic electron transfer resulting in the formation of radical anions. These radical anions react further following two divergent pathways: formation of amorphous carbon via ring-opening processes or hydride transfer reactions resulting in the formation of the diradical species benzyne and pyridyne. The former pathway is dominant for pyridine, while the latter is favored for benzene. These results have important implications for ongoing work in the areas of optoelectronic devices, interstellar chemistry, and catalysis.

ASSOCIATED CONTENT

Supporting Information

Tables of complete vibrational assignments for species discussed, and an additional figure of possible ring-opening degradation products for pyridine. This material is available free of charge via the Internet at http://pubs.acs.org.

AUTHOR INFORMATION

Corresponding Author

pembertn@u.arizona.edu

Present Address

[†]General Atomics Electronics Systems Inc., 4990 Greencraig Ln., San Diego, CA 92123

Notes

The authors declare no competing financial interest.

ACKNOWLEDGMENTS

These studies were supported as part of the Center for Interface Science: Solar Electric Materials, an Energy Frontier Research Center funded by the U.S. Department of Energy, Office of Science, Office of Basic Energy Sciences, under award number DE-SC0001084. The instrumentation for this work was supported by the National Science Foundation through grant awards CHE-0317114 and CHE-0848624. We gratefully acknowledge useful conversations with Professor Zhiping Zheng about metal−organic reaction chemistry relevant to these studies.

REFERENCES

(1) Cheng, X. *J. Mol. Struct. (THEOCHEM)* **2005**, *731*, 89−99.
(2) Liu, R.; Tate, D. R.; Clark, J. A.; Moody, P. R.; Van Buren, A. S.; Krauser, J. A. *J. Phys. Chem.* **1996**, *100*, 3430−3434.
(3) Wang, X.; Andrews, L. *J. Phys. Chem. A* **2004**, *108*, 11500−11510.
(4) Huang, J.-H.; Han, K.-L.; Zhu, R.-S.; He, G.-Z. *Spectrochim. Acta, Part A* **1999**, *55*, 1165−1175.
(5) Lapinski, A.; Spanget-Larsen, J.; Langgard, M.; Waluk, J.; Radziszewski, J. G. *J. Phys. Chem. A* **2001**, *105*, 10520−10524.
(6) Liu, R.; Zhou, X.; Pulay, P. *J. Phys. Chem.* **1992**, *96*, 8336−8339.
(7) Radziszewski, J. G.; Hess, B. A.; Zahradnik, R. *J. Am. Chem. Soc.* **1992**, *114*, 52−57.
(8) Weaver, S. L. W.; Remijan, A. J.; McMahan, R. J.; McCall, B. J. *Astrophys. J.* **2007**, *671*, L153−L156.
(9) Zhou, Z.; Sfeir, M. Y.; Zhang, L.; Hybertsen, M. S.; Steigerwald, M.; Brus, L. *Astrophys. J.* **2006**, *638*, L105−L108.
(10) Cernicharo, J.; Heras, A. M.; Tielens, A.; Pardo, J. R.; Herpin, F.; Guelin, M.; Waters, L. *Astrophys. J.* **2001**, *546*, L123−L126.
(11) Fries, M.; Steele, A. *Science* **2008**, *320*, 91−93.
(12) Sun, M.; Li, D.; Zheng, Y.; Zhang, W.; Shao, Y.; Chen, Y.; Li, W.; Fu, X. *Environ. Sci. Technol.* **2009**, *43*, 7877−7882.
(13) Hanusa, T. P. *Polyhedron* **1990**, *9*, 1345−1362.
(14) Fredriksson, C.; Stafstrom, S.; Dannetun, P.; Fauquet, C.; Salaneck, W. R.; Lazzaroni, R.; Bredas, J. L.; Ouhlal, A.; Selmani, A. *Plast. Eng.* **1998**, *43*, 199−211.
(15) Zhou, Y. L.; Lin, C. S.; Zhang, R. Q.; Wang, R. S. *J. Chem. Phys.* **2005**, *122*, 194322.
(16) *CRC Handbook of Chemistry and Physics*, 87th ed.; CRC Press: Boca Raton, FL, 2006.
(17) McKee, M. L. *J. Phys. Chem.* **1991**, *95*, 7247−7253.
(18) Kranokutski, S. A.; Yang, D.-S. J. *J. Chem. Phys.* **2009**, *130*, 134313−134321.
(19) Rodgers, M. T.; Stanley, J. R.; Amunugama, R. *J. Am. Chem. Soc.* **2000**, *122*, 10969−10978.
(20) Stossel, M.; Staudigel, J.; Steuber, F.; Simmerer, J.; Winnacker, A. *Appl. Phys. A: Mater. Sci. Process.* **1999**, *68*, 387−390.
(21) Davis, R. J.; Pemberton, J. E. *J. Phys. Chem. A* **2009**, *113*, 4397−4402.
(22) Davis, R. J.; Pemberton, J. E. *J. Am. Chem. Soc.* **2009**, *131*, 10009−10014.
(23) Davis, R. J.; Pemberton, J. E. *J. Phys. Chem. C* **2008**, *112*, 4364−4371.

(24) Schalnat, M. C.; Hawkridge, A. M.; Pemberton, J. E. *J. Phys. Chem. C* **2011**, *115*, 13717−13724.
(25) Matz, D. L.; Pemberton, J. E. *J. Phys. Chem. C* **2012**, *116*, 11548−11555.
(26) Hawkridge, A. M.; Pemberton, J. E. *J. Am. Chem. Soc.* **2002**, *125*, 624−625.
(27) Tiani, D. J.; Pemberton, J. E. *Langmuir* **2003**, *19*, 6422−6429.
(28) Goodman, D. W.; Madey, T. E.; Ono, M.; Yates, J. T. *J. Catal.* **1977**, 279−290.
(29) Ishii, K.; Nakayama, H.; Yoshida, T.; Usui, H.; Koyama, K. *Bull. Chem. Soc. Jpn.* **1996**, *69*, 2831−2838.
(30) Moskovits, M.; Dilella, D. P. *J. Chem. Phys.* **1980**, *73*, 6068−6075.
(31) Wolkow, R. A.; Moskovits, M. *J. Chem. Phys.* **1992**, *96*, 3966−3980.
(32) Petrie, S. *Int. J. Mass Spectrom.* **2003**, *227*, 33−46.
(33) Mochida, K.; Mizuno, Y. *Chem. Lett.* **1986**, *15*, 1125−1128.
(34) Mochida, K.; Takeuchi, K.; Hiraga, Y.; Ogawa, H. *Organometallics* **1987**, *6*, 2293−2297.
(35) Mochida, K.; Mizuno, Y. *Bull. Chem. Soc. Jpn.* **1987**, *60*, 273−276.
(36) Wenthold, P. G. *Angew. Chem., Int. Ed.* **2005**, *44*, 7170−7172.
(37) Zhang, X.; Maccarone, A. T.; Nimlos, M. R.; Kato, S.; Bierbaum, V. M.; Ellison, G. B.; Ruscic, B.; Simmonett, A. C.; Allen, W. D.; Schaefer, H. F. *J. Chem. Phys.* **2007**, *126*, 044312.
(38) Hajgato, B.; Deleuze, M. S.; Tozer, D. J.; De Proft, F. *J. Chem. Phys.* **2008**, *129*, 084308−15.
(39) Mitsui, M.; Nakajima, A.; Kaya, K.; Even, U. *J. Chem. Phys.* **2001**, *115*, 5707−5710.
(40) Leopold, D. G.; Miller, A. E. S.; Lineberger, W. C. *J. Am. Chem. Soc.* **1986**, *108*, 1379−1384.
(41) Hahn, J. R.; Kang, H. S. *Surf. Sci.* **2010**, *604*, 258−264.
(42) Vivoni, A.; Birke, R. L.; Foucault, R.; Lombardi, J. R. *J. Phys. Chem. B* **2003**, *107*, 5547−5557.
(43) Nenner, I.; Schulz, G. J. *J. Chem. Phys.* **1975**, *62*, 1747−1758.
(44) Han, S. Y.; Song, J. K.; Kim, J. H.; Oh, H. B.; Kim, S. K. *J. Chem. Phys.* **1999**, *111*, 4041−4050.
(45) Wang, D. S.; Han, K. L.; Yang, S. H. *Chin. J. Chem. Phys.* **2006**, *19*, 123−125.
(46) Kasai, P. H.; McLeod, D. *J. Am. Chem. Soc.* **1972**, *94*, 720−727.
(47) Shvartsburg, A. A. *Chem. Phys. Lett.* **2003**, *376*, 6−10.
(48) Solar, S.; Getoff, G.; Sehested, K.; Holcman, J. *Radiat. Phys. Chem.* **1993**, *41*, 825−834.
(49) Turecek, F.; Wolken, J. K.; Sadilek, M. *Eur. J. Mass Spectrom.* **1998**, *4*, 321−332.
(50) LaVerne, J. A.; Carmichael, I.; Araos, M. S. *J. Phys. Chem. A* **2005**, *109*, 461−465.
(51) Winkler, M.; Cakir, B.; Sander, W. *J. Am. Chem. Soc.* **2004**, *126*, 6135−6149.
(52) Cheng, X.; Niu, L.; Zhao, Y.; Zhao, Z. *Spectrochim. Acta, Part A* **2004**, *60*, 907−914.
(53) Cheng, X. L.; Zhao, Y. Y.; Zhou, Z. Y. *J. Mol. Struct. (THEOCHEM)* **2004**, *678*, 17−21.
(54) Liu, R.; Huang, T. T. S.; Tittle, J.; Xia, D. *J. Phys. Chem. A* **2000**, *104*, 8368−8374.
(55) Nam, H. H.; Leroi, G. E.; Harrison, J. F. *J. Phys. Chem.* **1991**, *95*, 6514−6519.
(56) Nam, H. H.; Leroi, G. E. *J. Am. Chem. Soc.* **1988**, *110*, 4096−4097.
(57) Ferrari, A. C.; Robertson, J. *Phys. Rev. B* **2000**, *61*, 14095−14107.
(58) Kozhevina, L. I.; Semenova, R. G.; Rybachenko, V. I.; Titov, E. V. *Ukrain. Chem. J.* **1986**, *52*, 736−742.
(59) Ervin, K. M.; DeTuri, V. F. *J. Phys. Chem. A* **2002**, *106*, 9947−9956.
(60) Friderichsen, A. V.; Radziszewski, J. G.; Nimlos, M. R.; Winter, P. R.; Dayton, D. C.; David, D. E.; Ellison, G. B. *J. Am. Chem. Soc.* **2001**, *123*, 1977−1988.
(61) Bauer, S. H.; Aten, C. F. *J. Chem. Phys.* **1963**, *39*, 1253−1260.
(62) Moskaleva, L. V.; Madden, L. K.; Lin, M. C. *Phys. Chem. Chem. Phys.* **1999**, *1*, 3967−3972.
(63) Davico, G. E.; Bierbaum, V. M.; DePuy, C. H.; Ellison, G. B.; Squires, R. R. *J. Am. Chem. Soc.* **1995**, *117*, 2590−2599.
(64) Madden, L. K.; Moskaleva, L. V.; Kristyan, S.; Lin, M. C. *J. Phys. Chem. A* **1997**, *101*, 6790−6797.
(65) Deng, W. Q.; Han, K. L.; Zhan, J. P.; He, G. Z. *Chem. Phys. Lett.* **1998**, *288*, 33−36.
(66) Stevenson, G. R.; Sturgeon, B. E.; Vines, K. S.; Peters, S. J. *J. Phys. Chem.* **1988**, *92*, 6850−6852.
(67) Stevenson, G. R.; Espe, M. P.; Reiter, R. C. *J. Am. Chem. Soc.* **1986**, *108*, 5760−5762.
(68) Frenklach, M.; Feigelson, E. D. *Astrophys. J.* **1989**, *341*, 372−384.
(69) Richter, H.; Howard, J. B. *Prog. Energy Combust.* **2000**, *26*, 565−608.
(70) Ishii, H.; Sugiyama, K.; Ito, E.; Seki, K. *Adv. Mater.* **1999**, *11*, 605−625.
(71) Xu, Q.; Ouyang, J.; Yang, Y.; Ito, T.; Kido, J. *Appl. Phys. Lett.* **2003**, *83*, 4695−4697.
(72) Jabbour, G. E.; Kawabe, Y.; Shaheen, S. E.; Wang, J. F.; Morrell, M. M.; Kippelen, B.; Peyghambarian, N. *Appl. Phys. Lett.* **1997**, *71*, 1762−1764.
(73) Kang, S. J.; Park, D. S.; Kim, S. Y.; Whang, C. N.; Jeong, K.; Im, S. *Appl. Phys. Lett.* **2002**, *81*, 2581−2583.
(74) Li, F.; Tang, H.; Anderegg, J.; Shinar, J. *Appl. Phys. Lett.* **1997**, *70*, 1233−1235.
(75) Piromreun, P.; Oh, H.; Shen, Y.; Malliaras, G. G.; Scott, J. C.; Brock, P. J. *Appl. Phys. Lett.* **2000**, *77*, 2403−2405.
(76) Stossel, M.; Staudigel, J.; Steuber, F.; Blassing, J.; Simmerer, J.; Winnacker, A. *Appl. Phys. Lett.* **2000**, *76*, 115−117.
(77) Stossel, M.; Staudigel, J.; Steuber, F.; Simmerer, J.; Winnacker, A.; Neuner, H.; Metzdorf, D.; Johannes, H. H.; Kowalsky, W. *Synth. Met.* **2000**, *111−112*, 19−24.
(78) Donley, C.; Dunphy, D.; Paine, D.; Carter, C.; Nebesny, K.; Lee, P.; Alloway, D.; Armstrong, N. R. *Langmuir* **2001**, *18*, 450−457.
(79) Ko, C. W.; Tao, Y. T. *Appl. Phys. Lett.* **2001**, *79*, 4234−4236.
(80) Koch, N. *ChemPhysChem* **2007**, *8*, 1438−1455.
(81) Ma, H.; Liu, M. S.; Jen, A. K. Y. *Polym. Int.* **2009**, *58*, 594−619.
(82) Kubicki, J. D.; Blake, G. A.; Apitz, S. E. *Environ. Toxicol. Chem.* **1999**, *18*, 1656−1662.
(83) Miller, J. H.; Andrews, P. A.; Lund, P. A.; Schatz, J. *J. Chem. Phys.* **1980**, *73*, 4932−4939.
(84) Munzel, N.; Schweig, A. *Chem. Phys. Lett.* **1988**, *147*, 192−194.
(85) Kikuchi, O.; Hondo, Y.; Morihashi, K.; Nakayama, M. *Bull. Chem. Soc. Jpn.* **1988**, *61*, 291−292.
(86) Guo, C.; Cao, Z.; Zhang, Q. *Chem. Phys. Lett.* **2004**, *386*, 448−453.